Acoustoelectric Non-Reciprocity in Lithium Niobate-on-Silicon Delay Lines

Hakhamanesh Mansoorzare, *Graduate Student Member, IEEE*, and Reza Abdolvand, *Senior Member, IEEE*

***Abstract*— Lamb wave delay lines with acoustoelectrically-induced non-reciprocity are demonstrated in suspended lithium niobate-on-silicon waveguides for the first time. An electric current is fed through the silicon layer in the same axis as the piezoelectrically-transduced acoustic waves which are attenuated or amplified depending on the direction of the energy exchange with drifting electrons (i.e. acoustoelectric (AE) effect). Therefore, the insertion loss (IL) and non-reciprocity of the delay line is adjustable by controlling the current bias which varies the electron drift velocity and the subsequent momentum transfer. Proof-of-concept delay lines in the range of 600 MHz to 700 MHz are demonstrated with a fractional bandwidth as high as 2.8% and AE gain as high as 5.6 dB resulting in ∼20 dB of non-reciprocity. These non-reciprocal components could offer a monolithic and dynamically-tunable solution to the numerous issues that arise from the increasing congestion and interferences in the telecommunication spectrum and suggests the possibility of developing fully-switchable low-IL delay lines through design/fabrication optimizations.**

***Index Terms*— Acoustoelectric, acoustic delay line, heterostructure, lamb wave, Lithium Niobate, non-reciprocal.**

I. Introduction

THE ever-increasing scarcity of the telecommunication spectrum has been calling for hardware architectures that could operate in full-duplex mode. However, enabling simultaneous transmission and reception, requires non-reciprocal components to be integrated in the telecommunication front-tend modules. While such components are typically realized by utilizing magnetic materials [1], the application of such devices is limited by the challenges in their integration and the cost considerations. Hence, alternative approaches have been studied in which non-linearity of media [2]–[4] or spatio-temporal modulation of a non-magnetic feature of the system is exploited. With regards to the latter, modulating the mechanical properties of the device [5] or introducing asymmetry in the system structure [6] have been examined as static (with respect to the signal path direction) solutions. In contrast, angular momentum biasing [7], [8] and the use of commuted networks [9], [10] were proposed as dynamic, multi-component, and more complex solutions.

In an alternative class of monolithic solutions, non-reciprocity is achieved through utilization of directional momentum exchange processes between phonons and photons [11], electrons and photons [12], and phonons and electrons [13]. The latter, known as the acoustoelectric (AE) effect, has been extensively demonstrated in surface acoustic wave (SAW) devices in the past [14]–[16] and more recently in lithium niobate (LN) [17]–[21] and gallium nitride (GaN) [22]–[24] heterostructures. Nonetheless, advancements in material growth and bonding have considerably facilitated the implementation of more efficient AE devices. In AE devices, the strain-induced perturbation of the bound electrons and drifting free electrons could lead to the amplification of the acoustic waves (AW) provided that the electron drift is in parallel with the AW and faster than its phase velocity (V_{AW}). Thus, the electromechanical coupling and the carrier mobility are the two most critical factors impacting the efficiency of the AE effect.

AE effect has been recently observed in composite aluminum nitride (AlN)-on-silicon (Si) cavities [25], [26] and AlN-on-germanium waveguides [27]. Motivated by the reported high coupling factors of fundamental symmetric Lamb waves (S_0) in suspended thin films of LN [28], [29], in this work we aim to demonstrate an acoustoelectrically-induced non-reciprocal response in suspended LN-Si delay lines. Benefiting from the large coupling of S_0 mode in LN-Si slab and relatively high electron drift velocity (V_d) in the lightly n-type doped Si layer, in such devices, a large fractional bandwidth (FBW) with strong non-reciprocity is postulated and observed. On the other hand, superior power handling of Si is believed to enable continuous wave (CW) operation of the device; a notable advantage over the implementations in which the injected current has to be pulsed to avoid nonlinearity [19], [20].

II. Design and Implementation

The AE efficiency is impacted by both piezoelectric and deformation potential couplings [30]. Thus, it is intensified by stronger penetration of the evanescent fields into the semiconductor and by inducing larger mechanical strains. Consequently, the lateral field excitation (LFE) of an AW with high electromechanical coupling in a composite piezoelectric-semiconductor slab is an appealing concept for implementation of an efficient AE device. It has been shown

Manuscript received June 22, 2020; accepted July 1, 2020. Date of publication July 6, 2020; date of current version August 26, 2020. This work was supported by the National Science Foundation (NSF) under Award 1810143. The review of this letter was arranged by Editor S. Pourkamali. *(Corresponding author: Hakhamanesh Mansoorzare.)*

The authors are with the Department of Electrical and Computer Engineering, University of Central Florida, Orlando, FL 32816 USA (e-mail: hakha@knights.ucf.edu).

Color versions of one or more of the figures in this letter are available online at http://ieeexplore.ieee.org.

Digital Object Identifier 10.1109/LED.2020.3007062

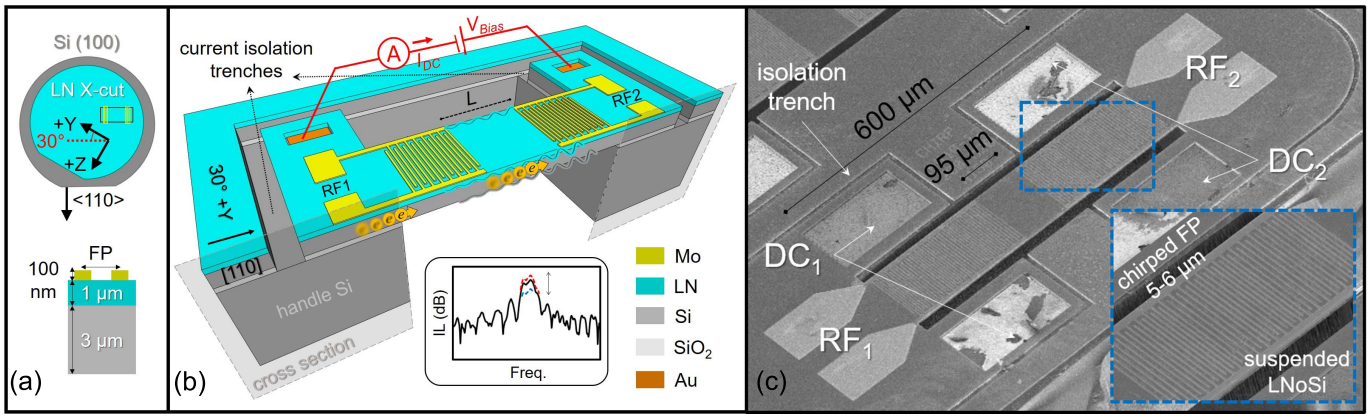

Fig. 1. (a) Bonding orientation of the LN-Si stack; (b) conceptual schematic of the device structure where the AWs launched by the IDTs will be amplified or attenuated by the electrons drifting in the Si layer; (c) the SEM of a fabricated prototype with the inset showing its chirped IDT pattern for achieving a wider FBW.

that d_{22} coupling constant of the X-cut LN reaches a large maximum once the main strain tensor (i.e. the 2 axis as in d_{22}) is oriented in line with the 30° off +y-axis [31]. We will exploit this large d_{22} to laterally excite the S_0 mode in a LN-Si acoustic waveguide. Accordingly, the device stack (provided by NGK Insulators) is formed by bonding an X-cut LN substrate onto a 3 μm (100) SOI and aligned with the <110> Si plane followed by thinning it down to 1 μm (as shown in Fig. 1 (a)).

100 nm thick interdigital transducers (IDT) excite and detect the AW between the 2 ports while the DC contacts to the underlying Si feed the drifting electrons. This current provides for directional AW amplification (same propagation direction) or attenuation (opposite propagation direction), resulting in non-reciprocity and switchability. The lateral boundary of the device is formed by etching the stack from top and the device is suspended by etching the backside handle layer. This will also restrict the current to only pass through the underlying Si body. The conceptual schematic and the scanning electron micrograph (SEM) of a fabricated prototype delay line are displayed in Fig. 1 (b) and (c), respectively.

The AE amplification coefficient (α) is analytically expressed in the form of

$$\alpha/k_0 = \frac{K^2}{2}\frac{\gamma\omega\tau}{1+(\gamma\omega\tau)^2} \quad (1)$$

with k_0 and ω being the wavenumber and angular frequency, K^2 the effective electromechanical coupling, γ the normalized difference between V_d and V_{AW} (i.e. $V_d/V_{AW}-1$), and τ the effective carrier relaxation time determined by the conductivity ($\sim \sigma^{-1}$) and permittivity ($\sim \varepsilon_{\text{effective}}$) of the structure [32]. The ideal value of K^2 can be approximated by the dispersion relation of the device stack as shown in Fig. 2 (a) and comparing V_{AW} for the free and metallized surface [33]. It is worth mentioning that the dependency of K^2 on the IDT finger pitch (FP $= \pi/k_0$) varies by the LN/Si thickness ratio. From (1) the theoretical value of α as the function of the applied drift field ($E_d = V_d \cdot \mu^{-1}$) is plotted in Fig. 2 (b) at FP $= 5$ μm. The doping of Si is swept from 1E14 to 1E15 cm^{-3} to account for the deviation of free electrons from the initial doping (n-type at 5E14 to 9E14 cm^{-3}) as a result of trap states especially at the LN-Si boundary. The relationship between α and E_d clearly

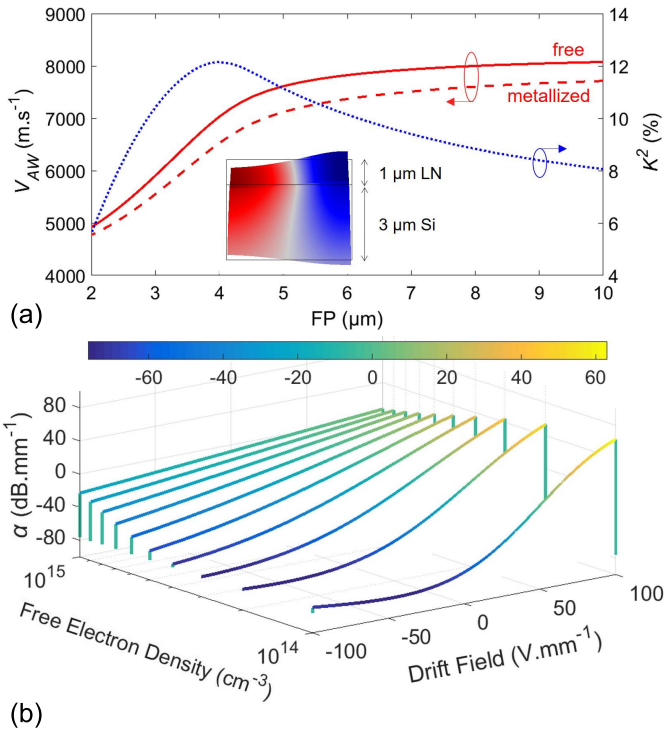

Fig. 2. (a) Dispersion characteristic of the LN-Si stack having free and metallized surface and the derived K^2 value; (b) theoretical value of α as a function of E_d for a range of free electron density.

depends on the density of free electrons and a larger gain for a lower E_d is observed at a lower range of density. For instance, at $E_d = 60$ V·mm^{-1} based on the initial doping range, an AE gain of 9.7 to 17.4 dB·mm^{-1} can be expected. Once α is fitted to the measurement data, a gain of 10.2 dB·mm^{-1} at the doping of 8.5E14 cm^{-3} is projected (see Fig. 4 (b) in the following section).

The passband response of the delay line is determined by mapping the spatial arrangement of the IDT into the frequency domain through the Fourier transform with its center frequency being determined by the IDT FP [34]. As such, a wide range of band pass responses can be implemented. Ideally, the AE gain selectively applies to the passband as only such AWs primarily propagate along the drifting electrons. This with a proper mode isolation could translate into an amplification

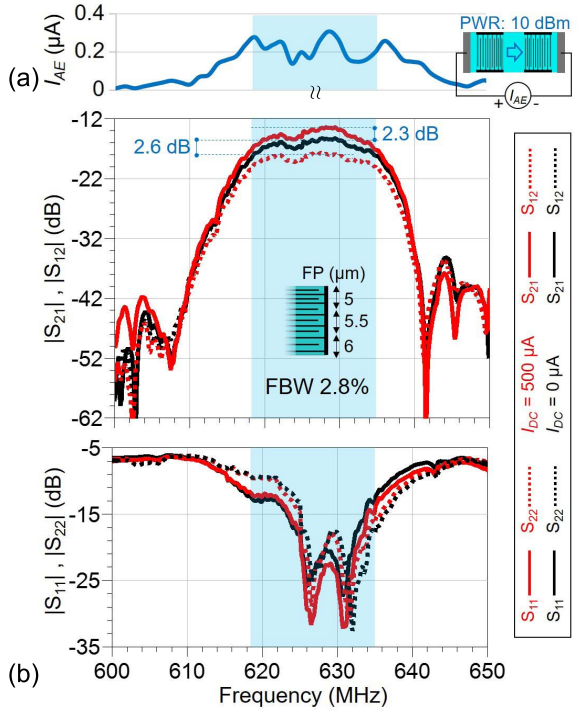

Fig. 3. (a) DC current generated as the input RF frequency is swept from 600 MHz to 650 MHz in a delay line with $L = 95$ μm; (b) the frequency response of the device showing the reciprocal response without passing a current (black) and the acoustoelectrically induced non-reciprocity (red). A CW current of 500 μA at E_d of 80 V.mm^{-1} (48 V) is recorded in this case, resulting in 24 mW power consumption.

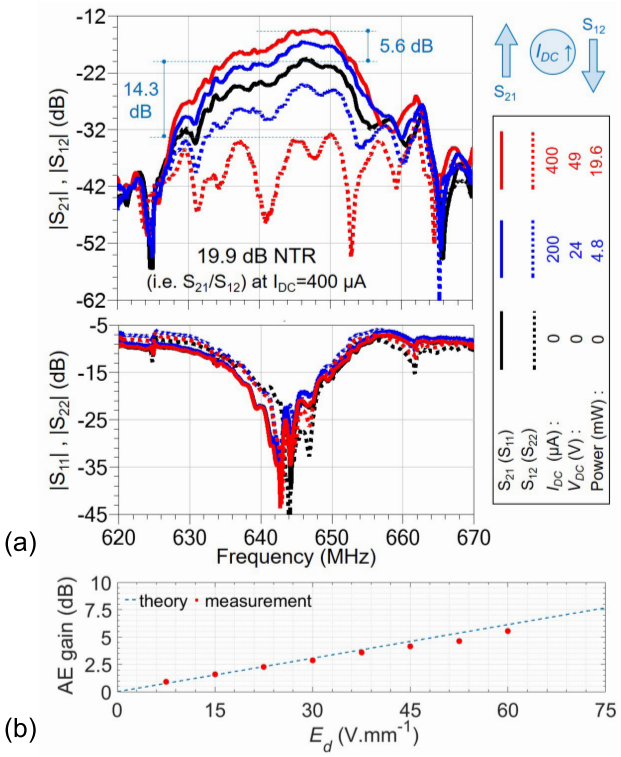

Fig. 4. (a) Measured frequency response of device with $L = 400$ μm for a current sweep, displaying switchable and tunable filtering; (b) the theoretical gain curve fitted to measurement results.

without degrading the signal to noise ratio (SNR) [35]. As the separation between the two ports ($L = 95$ and 400 μm here) is widened, AWs could undergo larger gain or loss, therefore, the attainable insertion loss (IL) tuning and the subsequent non-reciprocity is improved.

III. Measurement Results

The fabricated devices are characterized at room temperature and in atmospheric pressure by a vector network analyzer (Rhode & Schwarz ZNB 8) using ground signal ground (GSG) microprobes (Cascade Microtech Inc.); a short-open-load-thru calibration is performed to set the reference plane at the microprobe tips. At first, the AE effect is confirmed by measuring the acoustoelectrically generated DC current (I_{AE}) along the AW propagation. For this task, the Si contact pads are connected to a digital multimeter (Tektronix DM2510) and I_{AE} is recorded as the frequency of RF signal (at 10 dBm input power) is swept. I_{AE} is plotted in Fig. 3 (a) for a delay line with chirped IDTs (FP swept from 5 to 6 μm) in both ports that are 95 μm apart. Evidently, I_{AE} peaks almost exclusively within the passband of the delay line, reaching $\sim$0.3 μA. Fig. 3 (b) shows the RF characteristic of the delay line with the terminations conjugately matched to the impedance of the device ports; doing so compensates the mismatch loss by $\sim$3 dB and an IL of 15.2 dB is measured.

Next, E_d is applied across the DC contacts by means of a pair of DC probes connected to a power supply and the current (I_{DC}) passing through the underlying Si is measured. As the current value is increased, the otherwise reciprocal transmission (S_{21}) and reverse isolation (S_{12}) deviate from the initial condition. In the same direction as V_d, both S_{21} and S_{12} are concurrently improved and a gain of 2.3 dB with a nonreciprocal transmission ratio (NTR=S_{21}/S_{12}) of 4.9 dB is measured at a CW current of 500 μA and E_d of 80 V.mm^{-1} (48 V bias).

Finally, the tunability of the IL is demonstrated in Fig. 4 (a) by adjusting the I_{DC} in a device having the port IDTs (FP = 5 μm) 400 μm apart. As expected, a larger tuning range is realized as the current is swept from 0 to 400 μA and a 5.6 dB gain with 19.9 dB NTR is achieved at the maximum current (at 49 V bias and consuming 19.6 mW). The transmission direction is reversed by reversing I_{DC}, therefore, transmission can be suppressed close to the noise floor, virtually switching the device off. Furthermore, the impact of the AE amplification and attenuation is much more evident in the passband of the delay line. The measured AE gain in this case as a function of E_d is plotted in Fig 4 (b) along with the fitted theoretical values.

IV. Conclusion

Acoustoelectric (AE) effect was efficiently induced in Lamb wave acoustic waveguides fabricated on lithium niobate-on-silicon heterostructures to realize monolithic and dynamic non-reciprocal delay lines. Due to the direction and intensity-dependent impact of drifting electrons on the acoustic phonons, the insertion loss and non-reciprocity of the device could be tuned. The selective AE amplification of the signals within the passband suggests the possibility of preserving (and even improving) the signal to noise ratio while opting for larger LN/Si thickness ratios could significantly improve the attainable bandwidth, gain, and non-reciprocity.

REFERENCES

[1] J. D. Adam, L. E. Davis, G. F. Dionne, E. F. Schloemann, and S. N. Stitzer, "Ferrite devices and materials," *IEEE Trans. Microw. Theory Techn.*, vol. 50, no. 3, pp. 721–737, Mar. 2002, doi: 10.1109/22.989957.

[2] B. Liang, B. Yuan, and J.-C. Cheng, "Acoustic diode: Rectification of acoustic energy flux in one-dimensional systems," *Phys. Rev. Lett.*, vol. 103, no. 10, Sep. 2009, Art. no. 104301, doi: 10.1103/PhysRevLett.103.104301.

[3] K. J. Moore, J. Bunyan, S. Tawfick, O. V. Gendelman, S. Li, M. Leamy, and A. F. Vakakis, "Nonreciprocity in the dynamics of coupled oscillators with nonlinearity, asymmetry, and scale hierarchy," *Phys. Rev. E, Stat. Phys. Plasmas Fluids Relat. Interdiscip. Top.*, vol. 97, no. 1, Jan. 2018, Art. no. 012219, doi: 10.1103/PhysRevE.97.012219.

[4] L. Shao, W. Mao, S. Maity, N. Sinclair, Y. Hu, L. Yang, and M. Lončar, "Non-reciprocal transmission of microwave acoustic waves in nonlinear parity–time symmetric resonators," *Nature Electron.*, vol. 3, no. 5, pp. 267–272, May 2020, doi: 10.1038/s41928-020-0414-z.

[5] M. B. Zanjani, A. R. Davoyan, A. M. Mahmoud, N. Engheta, and J. R. Lukes, "One-way phonon isolation in acoustic waveguides," *Appl. Phys. Lett.*, vol. 104, no. 8, Feb. 2014, Art. no. 081905, doi: 10.1063/1.4866590.

[6] M. Ghatge, G. Walters, T. Nishida, and R. Tabrizian, "A non-reciprocal filter using asymmetrically transduced micro-acoustic resonators," *IEEE Electron Device Lett.*, vol. 40, no. 5, pp. 800–803, May 2019, doi: 10.1109/LED.2019.2907089.

[7] D. L. Sounas, C. Caloz, and A. Alù, "Giant non-reciprocity at the subwavelength scale using angular momentum-biased metamaterials," *Nature Commun.*, vol. 4, no. 1, p. 2407, Dec. 2013, doi: 10.1038/ncomms3407.

[8] C. Cassella, G. Michetti, M. Pirro, Y. Yu, A. Kord, D. L. Sounas, A. Alù, and M. Rinaldi, "Radio frequency angular momentum biased quasi-LTI nonreciprocal acoustic filters," *IEEE Trans. Ultrason., Ferroelectr., Freq. Control*, vol. 66, no. 11, pp. 1814–1825, Nov. 2019, doi: 10.1109/TUFFC.2019.2931121.

[9] N. Reiskarimian and H. Krishnaswamy, "Magnetic-free non-reciprocity based on staggered commutation," *Nature Commun.*, vol. 7, no. 1, pp. 1–10, Sep. 2016, doi: 10.1038/ncomms11217.

[10] R. Lu, T. Manzaneque, Y. Yang, L. Gao, A. Gao, and S. Gong, "A radio frequency nonreciprocal network based on switched acoustic delay lines," *IEEE Trans. Microw. Theory Techn.*, vol. 67, no. 4, pp. 1516–1530, Apr. 2019, doi: 10.1109/TMTT.2019.2895577.

[11] D. B. Sohn, S. Kim, and G. Bahl, "Time-reversal symmetry breaking with acoustic pumping of nanophotonic circuits," *Nature Photon.*, vol. 12, no. 2, pp. 91–97, Feb. 2018, doi: 10.1038/s41566-017-0075-2.

[12] H. Lira, Z. Yu, S. Fan, and M. Lipson, "Electrically driven nonreciprocity induced by interband photonic transition on a silicon chip," *Phys. Rev. Lett.*, vol. 109, no. 3, Jul. 2012, Art. no. 033901, doi: 10.1103/PhysRevLett.109.033901.

[13] Y. V. Gulyaev and V. I. Pustovoĭt, "Amplification of surface waves in semiconductors," *Sov. Phys. JETP* vol. 20, no. 6, p. 1508, 1965.

[14] R. M. White and F. W. Voltmer, "Ultrasonic surface-wave amplification in cadmium sulfide," *Appl. Phys. Lett.*, vol. 8, no. 2, pp. 40–42, Jan. 1966, doi: 10.1063/1.1754472.

[15] J. H. Collins, K. M. Lakin, C. F. Quate, and H. J. Shaw, "Amplification of acoustic surface waves with adjacent semiconductor and piezoelectric crystals," *Appl. Phys. Lett.*, vol. 13, no. 9, pp. 314–316, Nov. 1968, doi: 10.1063/1.1652628.

[16] G. S. Kino, "Acoustoelectric interactions in acoustic-surface-wave devices," *Proc. IEEE*, vol. 64, no. 5, pp. 724–748, May 1976, doi: 10.1109/PROC.1976.10202.

[17] C. P. Carmichael, M. S. Smith, A. R. Weeks, and D. C. Malocha, "Experimental investigation of surface acoustic wave acoustoelectric effect using a graphene film on lithium niobate," *IEEE Trans. Ultrason., Ferroelectr., Freq. Control*, vol. 65, no. 11, pp. 2205–2207, Nov. 2018, doi: 10.1109/TUFFC.2018.2870042.

[18] U. K. Bhaskar, S. A. Bhave, and D. Weinstein, "Silicon acousto-electronics with thin film lithium niobate," *J. Phys. D, Appl. Phys.*, vol. 52, no. 5, Jan. 2019, Art. no. 05LT01, doi: 10.1088/1361-6463/aaee59.

[19] L. Hackett, A. Siddiqui, D. Dominguez, J. K. Douglas, A. Tauke-Pedretti, T. Friedmann, G. Peake, S. Arterburn, and M. Eichenfield, "High-gain leaky surface acoustic wave amplifier in epitaxial InGaAs on lithium niobate heterostructure," *Appl. Phys. Lett.*, vol. 114, no. 25, Jun. 2019, Art. no. 253503, doi: 10.1063/1.5108724.

[20] A. M. Siddiqui, L. P. Hackett, D. Dominguez, A. Tauke-Pedretti, T. Friedmann, G. Peake, M. R. Miller, J. K. Douglas, and M. Eichenfield, "Large acoustoelectric effect in wafer bonded indium gallium arsenide/lithium niobate heterostructure augmented by novel gate control," in *Proc. 20th Int. Conf. Solid-State Sens., Actuators Microsyst. Eurosensors (TRANSDUCERS EUROSENSORS)*, Jun. 2019, pp. 61–64, doi: 10.1109/TRANSDUCERS.2019.8808281.

[21] S. Ghosh, "FDSOI on lithium niobate using Al_2O_3 wafer-bonding for acoustoelectric RF microdevices," in *Proc. 20th Int. Conf. Solid-State Sens., Actuators Microsyst. Eurosensors (TRANSDUCERS EUROSENSORS)*, 2019, pp. 535–538, doi: 10.1109/TRANSDUCERS.2019.8808600.

[22] H. Zhu and M. Rais-Zadeh, "Non-reciprocal acoustic transmission in a GaN delay line using the acoustoelectric effect," *IEEE Electron Device Lett.*, vol. 38, no. 6, pp. 802–805, Jun. 2017, doi: 10.1109/LED.2017.2700013.

[23] S. Ghosh, T. Hancock, M. Storey, L. Parameswaran, M. Geis, R. Ralston, and D. Weinstein, "Nonreciprocal acoustoelectric interaction of surface waves and fluorine plasma-treated AlGan/GaN 2DEG," in *Proc. 19th Int. Conf. Solid-State Sens., Actuators Microsyst. (TRANSDUCERS)*, Jun. 2017, pp. 1939–1942, doi: 10.1109/TRANSDUCERS.2017.7994448.

[24] S. Ghosh, M. A. Hollis, and R. J. Molnar, "Acoustoelectric amplification of Rayleigh waves in low sheet density AlGaN/GaN heterostructures on sapphire," *Appl. Phys. Lett.*, vol. 114, no. 6, Feb. 2019, Art. no. 063502, doi: 10.1063/1.5080450.

[25] H. Mansoorzare, R. Abdolvand, and H. Fatemi, "Investigation of phonon-carrier interactions in silicon-based MEMS resonators," in *Proc. IEEE Int. Freq. Control Symp. (IFCS)*, May 2018, pp. 1–3, doi: 10.1109/FCS.2018.8597526.

[26] H. Mansoorzare and R. Abdolvand, "Acoustoelectric amplification in lateral-extensional composite piezo-silicon resonant cavities," in *Proc. Joint Conf. IEEE Int. Freq. Control Symp. Eur. Freq. Time Forum (EFTF/IFC)*, Apr. 2019, pp. 1–3, doi: 10.1109/FCS.2019.8856012.

[27] F. Hakim, M. Ramezani, S. Rassay, and R. Tabrizian, "Non-reciprocal acoustoelectric amplification in germanium-based Lamb wave delay lines," in *IEDM Tech. Dig.*, Dec. 2019, pp. 6–9, doi: 10.1109/IEDM19573.2019.8993543.

[28] S. Gong and G. Piazza, "Design and analysis of Lithium–Niobate-based high electromechanical coupling RF-MEMS resonators for wideband filtering," *IEEE Trans. Microw. Theory Techn.*, vol. 61, no. 1, pp. 403–414, Jan. 2013, doi: 10.1109/TMTT.2012.2228671.

[29] R. Lu, T. Manzaneque, Y. Yang, M.-H. Li, and S. Gong, "Gigahertz low-loss and wideband S0 mode lithium niobate acoustic delay lines," *IEEE Trans. Ultrason., Ferroelectr., Freq. Control*, vol. 66, no. 8, pp. 1373–1386, Aug. 2019, doi: 10.1109/TUFFC.2019.2916259.

[30] M. Pomerantz, "Ultrasonic loss and gain mechanisms in semiconductors," *Proc. IEEE*, vol. 53, no. 10, pp. 1438–1451, Oct. 1965, doi: 10.1109/PROC.1965.4258.

[31] I. E. Kuznetsova, B. D. Zaitsev, S. G. Joshi, and I. A. Borodina, "Investigation of acoustic waves in thin plates of lithium niobate and lithium tantalate," *IEEE Trans. Ultrason., Ferroelectr., Freq. Control*, vol. 48, no. 1, pp. 322–328, Jan. 2001, doi: 10.1109/58.896145.

[32] R. Adler, "Simple theory of acoustic amplification," *IEEE Trans. Sonics Ultrason.*, vol. SU-18, no. 3, pp. 115–118, Jul. 1971, doi: 10.1109/T-SU.1971.29605.

[33] S. G. Joshi and Y. Jin, "Electromechanical coupling coefficients of ultrasonic Lamb waves," *J. Acoust. Soc. Amer.*, vol. 94, no. 1, pp. 261–267, Jul. 1993, doi: 10.1121/1.407084.

[34] G. Matthaei, "Acoustic surface-wave transversal filters," *IEEE Trans. Circuit Theory*, vol. CT-20, no. 5, pp. 459–470, Sep. 1973, doi: 10.1109/TCT.1973.1083750.

[35] J. M. L. Miller, A. Ansari, D. B. Heinz, Y. Chen, I. B. Flader, D. D. Shin, L. G. Villanueva, and T. W. Kenny, "Effective quality factor tuning mechanisms in micromechanical resonators," *Appl. Phys. Rev.*, vol. 5, no. 4, Dec. 2018, Art. no. 041307, doi: 10.1063/1.5027850.